JACS
JOURNAL OF THE AMERICAN CHEMICAL SOCIETY

pubs.acs.org/JACS

Article

Influence of Solvent on Selective Catalytic Reduction of Nitrogen Oxides with Ammonia over Cu-CHA Zeolite

Jamal Abdul Nasir,* Jingcheng Guan, Thomas W. Keal, Alec W. Desmoutier, You Lu, Andrew M. Beale, C. Richard A. Catlow,* and Alexey A. Sokol*

Cite This: *J. Am. Chem. Soc.* 2023, 145, 247−259

Read Online

ACCESS | Metrics & More | Article Recommendations | Supporting Information

ABSTRACT: The copper-exchanged zeolite Cu-CHA has received considerable attention in recent years, owing to its application in the selective catalytic reduction (SCR) of NO_x species. Here, we study the NH_3-SCR reaction mechanism on Cu-CHA using the hybrid quantum mechanical/molecular mechanical (QM/MM) technique and investigate the effects of solvent on the reactivity of active Cu species. To this end, a comparison is made between water- and ammonia-solvated and bare Cu species. The results show the promoting effect of solvent on the oxidation component of the NH_3-SCR cycle since the formation of important nitrate species is found to be energetically more favorable on the solvated Cu sites than in the absence of solvent molecules. Conversely, both solvent molecules are predicted to inhibit the reduction component of the NH_3-SCR cycle. Diffuse reflectance infrared fourier-transform spectroscopy (DRIFTS) experiments exploiting (concentration) modulation excitation spectroscopy (MES) and phase-sensitive detection (PSD) identified spectroscopic signatures of Cu-nitrate and Cu-nitrosamine (H_2NNO), important species which had not been previously observed experimentally. This is further supported by the QM/MM-calculated harmonic vibrational analysis. Additional insights are provided into the reactivity of solvated active sites and the formation of key intermediates including their formation energies and vibrational spectroscopic signatures, allowing the development of a detailed understanding of the reaction mechanism. We demonstrate the role of solvated active sites and their influence on the energetics of important species that must be explicitly considered for an accurate understanding of NH_3-SCR kinetics.

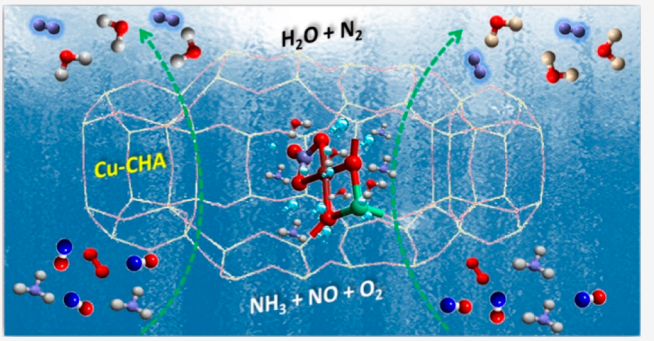

1. INTRODUCTION

Atmospheric NOx emissions, consisting mainly of NO, NO_2, and N_2O, are highly damaging to the environment, producing smog and acid rain; they are also "greenhouse gases" and pose a serious hazard to human health both through direct exposure and *via* the formation of ozone.[1,2] Human activity has had a dramatic impact on NOx levels through fossil fuel combustion, which releases both NO and NO_2 into the atmosphere.[3] To mitigate this problem, transition metal catalysis can be harnessed to remove NOx efficiently from exhaust gases through the selective catalytic reduction (SCR) reaction, in which ammonia is used to reduce these species to nitrogen.[4,5] The major exhaust gases from diesel engines are NO (>90%) rather than NO_2; therefore, the reduction of NOx occurs mostly *via* what is known as the "standard SCR" reaction.[6]

Small-pore zeolites containing copper such as Cu-SSZ-13, possessing the chabazite (CHA) topology, have shown outstanding performance in the NH_3-SCR reaction.[2,7,8] It has been reported that Cu-CHA has not only several active sites, including Cu^+ and Cu^{2+} ions in NH_3-SCR, but also species beyond single ions and with higher Cu-ion nuclearity.[9,10] For low-temperature SCR (<200−250 °C), it has been proposed that Cu ions of higher nuclearity are active, which is, however, not the case for high-temperature SCR where ions of low nuclearity have been proposed.[11] In the NH_3-SCR cycle, the reaction follows either a standard SCR (eq 1) or NO-activation pathway (eq 2), which can proceed with the same reduction step as the fast-SCR (eq 3); however, in the "NO-activation" cycle, the rate does not depend on the concentration of NO_2, while it is dependent on the concentration of NO_2 in the fast SCR.[12]

$$4NO + 4NH_3 + O_2 \rightarrow 4N_2 + 6H_2O \quad (1)$$

$$3NO + 2NH_3 + O_2 \rightarrow 2N_2 + 3H_2O + NO_2 \quad (2)$$

Received: September 14, 2022
Published: December 22, 2022

$$NO + 2NH_3 + NO_2 \rightarrow 4N_2 + 3H_2O \quad (3)$$

Water and ammonia vapors are among the key components of the NOx-containing exhaust gases, and their inevitable presence could lead to adsorption on the transition metal sites, affecting the energetics of the intermediate species.[13,14] Liu *et al.*[15] investigated the effect of water on NH_3-SCR activity over Cu-LTA and found a promoting effect of water on low-temperature SCR activity with a plausible solvated $[H_2O-Cu-NH_3]^+$ species. Similarly, the experimental study by Yu *et al.*[16] over Cu-SAPO-34 also showed a promoting effect of water and reported that in its presence, the reducibility of Cu^{2+} species at high temperature is improved, while NH_3 oxidation is inhibited. It is also found that ammonia does not block the formation of nitrates when water is present in the feed, as reported by Lee *et al.*[17] Moreover, some studies show that enhanced Cu-ion mobility is caused by ligating water and ammonia molecules, leading to better low-temperature NH_3-SCR activity.[10,15,18]

To optimize the catalytic process, not only the chemistry of active sites and the intrinsic NH_3–NO reaction kinetics need careful attention but also the diffusion of the counterion must be understood, which is strongly affected by the ligation of solvent molecules such as H_2O and NH_3. Generally, Al sites are responsible for restricting the mobility of counterions, due to electrostatic attraction to the framework. $[Cu(NH_3)_2]^+$ mobility inside the CHA framework at the sub-second time scale is predicted by Paolucci *et al.*[10] who found a displacement of 9 Å for $[Cu(NH_3)_2]^+$ by *ab initio* metadynamics. Furthermore, employing molecular dynamics (MD) simulation, O'Malley *et al.* found that the strong coordination of NH_3 with Cu^{2+} in the center of the CHA cage hinders the interaction of other molecules with the Cu sites.[19]

It is possible to split the NH_3-SCR redox cycle and separate the oxidation from the reduction step, which is achieved experimentally by switching between NH_3 + NO and NO + O_2[19] atmospheres to study the individual half-cycles.[12] The Cu(II)-nitrate species formed as a result of the NO + O_2 oxidation process can be converted back to the Cu(I) state under NH_3 + NO reductive conditions (Figure 1).

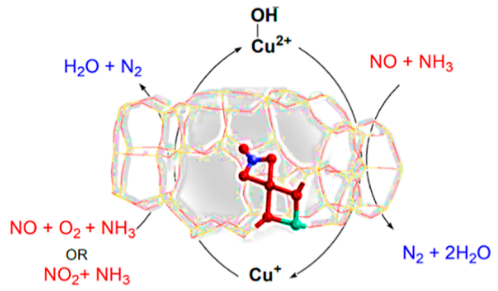

Figure 1. Schematic representation of the catalytic cycle of NH_3-SCR of NO_x.

Furthermore, NO can react with the nitrate intermediate to generate gaseous NO_2 and Cu-nitrite species. Such NO activation, which has been reported for both single Cu-sites and Cu(II)-pair-mediated systems, accounts for Cu(II) reduction and is often considered necessary for the NH_3-SCR reaction.[5,20] The formation of NO_2 species facilitates the oxidation half-cycle and hence leads to establishing a link to the fast SCR reaction.[21]

To understand how solvated Cu cations can control nitrogen chemistry in CHA zeolite, we investigate reaction mechanisms with both modeling and experimental techniques. For this purpose, we have employed density functional theory (DFT) using a quantum mechanical/molecular mechanical (QM/MM) methodology, as implemented in the ChemShell software, and DRIFTS which allow us to observe the formation and consumption of short-lived intermediates in the catalytic reaction. Hereby, we elucidate the influence of physisorbed solvents on the reactivity of Cu-CHA sites and their effect on the energetics of intermediates. We report a comprehensive study in which the computational analysis provides a clear assignment of all main spectroscopic features of the NH_3-SCR catalytic cycle, which are in good agreement with experiment. Thus, our investigation provides new insights into the NH_3-SCR reaction by understanding the chemistry of the solvated-Cu-CHA sites and their impact on the key steps in the reaction.

2. METHODS

2.1. QM/MM Methodologies. A hybrid QM/MM approach[22,23] using the ChemShell software[24−26] was employed to study the NH_3-SCR process over Cu-CHA. The model involves a quantum mechanical description of a relatively small cluster of ∼200 atoms around the reaction site, embedded in a much larger cluster modeled using a classical molecular mechanics forcefield. This approach is well suited for describing a local active site, as an alternative periodic DFT approach would require a large, supercell calculation to avoid spurious interactions between the periodically repeated reaction sites. It is also more straightforward in a non-periodic model to increase the accuracy of the QM description through the use of hybrid DFT functionals, as in the current study. Furthermore, the description of the electrostatic environment is more efficiently handled in the QM/MM model through a combination of MM atoms and point charges as detailed below.

In our CHA-cluster model, we set an active region, where all constituent atoms are allowed to relax freely, extending to a radius of 15 Å (∼28.3 Bohr) from the chosen center containing the Al site. A central core of 143 framework atoms and a charge-balancing Cu cation (not including hydrogen link atoms) is described at the QM level (Figure 2). The active region is in turn surrounded by a frozen spherical layer with a thickness of *ca.* 15 Å. The total number of atoms in the model is 6007, of which 700 are active. A judicious choice of the basis set discussed further below allows us to employ moderate basis sets in the QM region; for example, in the nitrate case, there are 2983 and 2797 Cartesian and harmonic basis functions, respectively, for the largest systems of interest (containing intermediate reacting species). The calculations for the QM clusters were performed using the GAMESS-UK package,[27] while for the MM part, the DL_POLY package[28] was employed, with the Hill-Sauer molecular mechanical forcefield,[29] which assumes that the atoms bind to each other by polar covalent bonds. Further we introduced the outer shell of point charges whose values have been fitted to reproduce accurately the electrostatic field in the active region of the infinite CHA-zeolite framework.

Atoms at the interface between QM and MM regions are connected by bonds that need careful treatment including terminating the QM region by adding hydrogen atoms, forming O-H groups, and use of modified MM charges at the boundary.[23,26] We divided the QM region into two parts and employed a dual basis set strategy: the number of atoms in the innermost QM1 region is ∼28 including the intermediates which are treated with the triplet-ζ basis set def2-TZVP,[30] while the outer QM2 region (115 atoms), which includes the terminating link H atoms, is treated with a smaller split valence with polarization def2-SVP[30] basis set. To build the QM/MM model, it is necessary to remove the classical charges from the QM centers and make sure that the total charge removed from the system is the

https://doi.org/10.1021/jacs.2c09823
J. Am. Chem. Soc. 2023, 145, 247−259

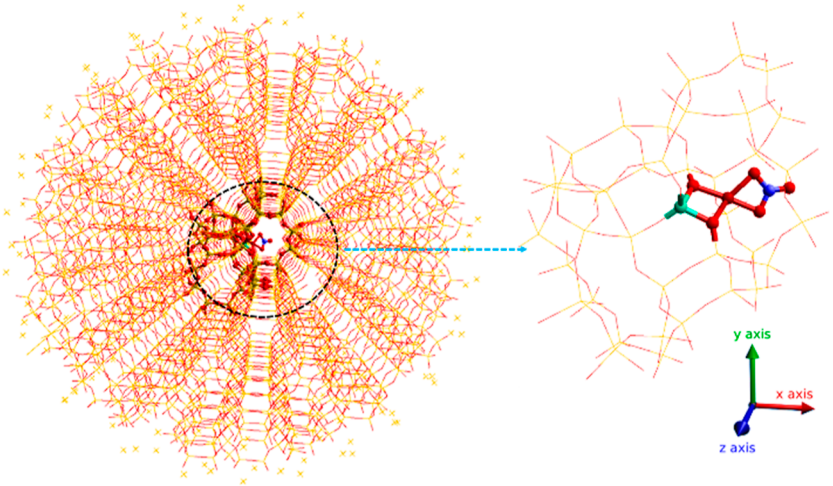

Figure 2. QM/MM embedding setup; CHA cluster (left) with a quantum mechanical region containing nitrate species (right). The outermost region contains point charges to ensure that the Madelung potential in the center of the cluster is accurately reproduced. Atom color codes: Cu (brown), Al (green), Si (yellow), O (red), N (blue), and H (white).

same as the total charge of the QM region. The guest species of interest in the zeolite and reactant gaseous species were also treated at the QM level using the higher quality def2-TZVP basis set. The coordinates of all atoms in the QM region and active MM region were fully optimized. To find the most favorable location of $Cu^{2+}-OH^{-}$ in Cu-CHA, we performed DFT calculations using a range of exchange–correlation density functionals, as presented in the Supporting Information section, and have selected the B97-2[31] results as providing the most accurate reaction energies and molecular structures. Therefore, the B97-2 data will be used in the main body of this paper. In particular, we have found that the extraframework Cu ions are more stable in eight-membered rings (8-MR) than 6-MR, by 0.3 eV (*cf.* a similar finding in ref 32). Considering that adsorbed molecules can diffuse through the larger channels, all the adsorbed species including the intermediates were placed within (or near) the 8-MR of the CHA cage. The water (O-end) and ammonia (N-end) molecules were placed at a distance of 2 Å from the Cu center with the proton pointing away from the adjacent oxygens and intermediate species to avoid artificial trapping in hydrogen-bonding interactions. We note that hydrogen bonding with framework oxygen can influence chemistry at metal sites by affecting the binding of functionally important $Cu-H_2O/NH_3$ units.

For vibrational frequencies at a local active site modeled by the hybrid QM/MM approach, only nuclear displacements of the active sites are included, that is, a frozen phonon approximation from the expanded environment accounting for electrostatic interactions is applied throughout the vibrational calculations. To this aim, we chose an active region that contains atoms around the Al center within three coordination spheres (5T-site), including the atoms of the intermediate species, and calculated normal and localized modes. Full details of the approach used for vibrational frequency calculations are given in the Supporting Information section.

2.2. Choice of the Model Cluster. To perform the QM/MM calculation, we first created a spherical embedded-cluster model (Figure 2) of CHA from the unit cell of siliceous CHA[33] optimized at the MM level using the GULP package.[34] After creating a simple CHA-cluster model, we constructed active sites. For example, in the case of a Brønsted acid site, we replaced one Si with Al and added a charge compensating proton on a neighboring oxygen atom at a site where it is most accessible to facilitate the reaction. The QM region which is contained within the active part of the model includes atoms from the third oxygen shell from the central T-site; as noted, we have added the hydrogen (link atoms) to saturate the terminal oxygen atoms. Furthermore, we modified the same cluster by incorporating copper into the cage of the CHA framework.

We first optimized the purely siliceous CHA cluster using ChemShell and employed the hybrid QM/MM model for zeolites developed by Sherwood.[35] The geometrical parameters obtained for the Si-tetrahedral sites by ChemShell employing two representative DFT functionals, B97-2[31] and BB1K,[36] were found to be in an accordance with the experimental data (details are in Supporting Information, Tables S1 and S2).

2.3. Catalyst Preparation. Synthesis of SSZ-13 zeolite (Si/Al = 13) was performed as reported earlier following the hydrothermal approach.[37] The *N,N,N* trimethyladamantammonium hydroxide was used as a structure-directing agent under fluoride media. The protonated zeolite is obtained by calcining the sample in the air, first for 2.5 h at 1 °C min^{-1} to 120 °C and then for 10 h at 4 °C min^{-1} to 550 °C. By employing the wet ion-exchange methodology, a typical amount of H-SSZ-13 is then mixed with a copper sulfate solution (50 mL of a 0.1 M solution of $CuSO_4$ per gram of zeolite) under constant heating (80 °C for 2 h) and stirring. The resultant product consists of a well-defined crystal of rhombohedral morphology (2.92 wt % Cu loading) which was washed with water and kept at 80 °C overnight.[38] To perform operando spectroscopic analysis, the pellets of zeolite (8 mm bore, 1.5-tonne pressure) were prepared which were then crushed and sieved to retain a 250–450 μm fraction for experiments.

2.4. Catalyst Characterization. Powder X-ray Diffraction (PXRD) patterns were collected to confirm phase purity and crystallinity on a Rigaku Miniflex diffractometer (Cu Kα_1, 1.54056 Å), and samples were loaded onto a flat Teflon sample holder. Diffraction patterns were collected between 5.0 and 50.0° in 0.02° steps. PXRD shows that a highly crystalline pure phase of Cu-SSZ-13 is present after calcination, subsequent ion-exchange, and calcination steps (see Figure S6). Energy-dispersive X-ray (EDX) analysis of Cu-SSZ-13 (see Table S19) shows that Cu-SSZ-13 has a composition of 2.92 wt % Cu with a Si/Al = 13 which represents 75% Cu ions exchanged into available H^+ sites. The Brunauer–Emmett–Teller (BET) method was used in the analysis of the total surface area, and the *t*-plot method was used in the micropore volume (Table S20).

2.5. DRIFTS Operando ME Experiments. DRIFTS spectra were recorded on a Bruker Vertex 70 spectrometer equipped with a liquid-N_2 cooled HgCdTe detector and a Praying Mantis mirror unit (Harrick). The spectroscopic cell connected to heated gas supply lines was equipped with a flat CaF_2 window (2 mm thick; diameter 25 mm). The outlet of the cell was coupled to a Fourier Transform Infrared (FTIR) spectrometer equipped with a 70 mm path length gas cell heated to 150 °C (Bruker Alpha). The sample was placed in the sample cup of the cell (*ca.* 30 mg, 57 mm^3) after being dried *in situ* in 10 vol % O_2/N_2 (100 mL min^{-1}) at 400 °C for 2 h. DRIFTS spectra were collected by accumulating 10 interferograms under 80 kHz

https://doi.org/10.1021/jacs.2c09823
J. Am. Chem. Soc. 2023, 145, 247–259

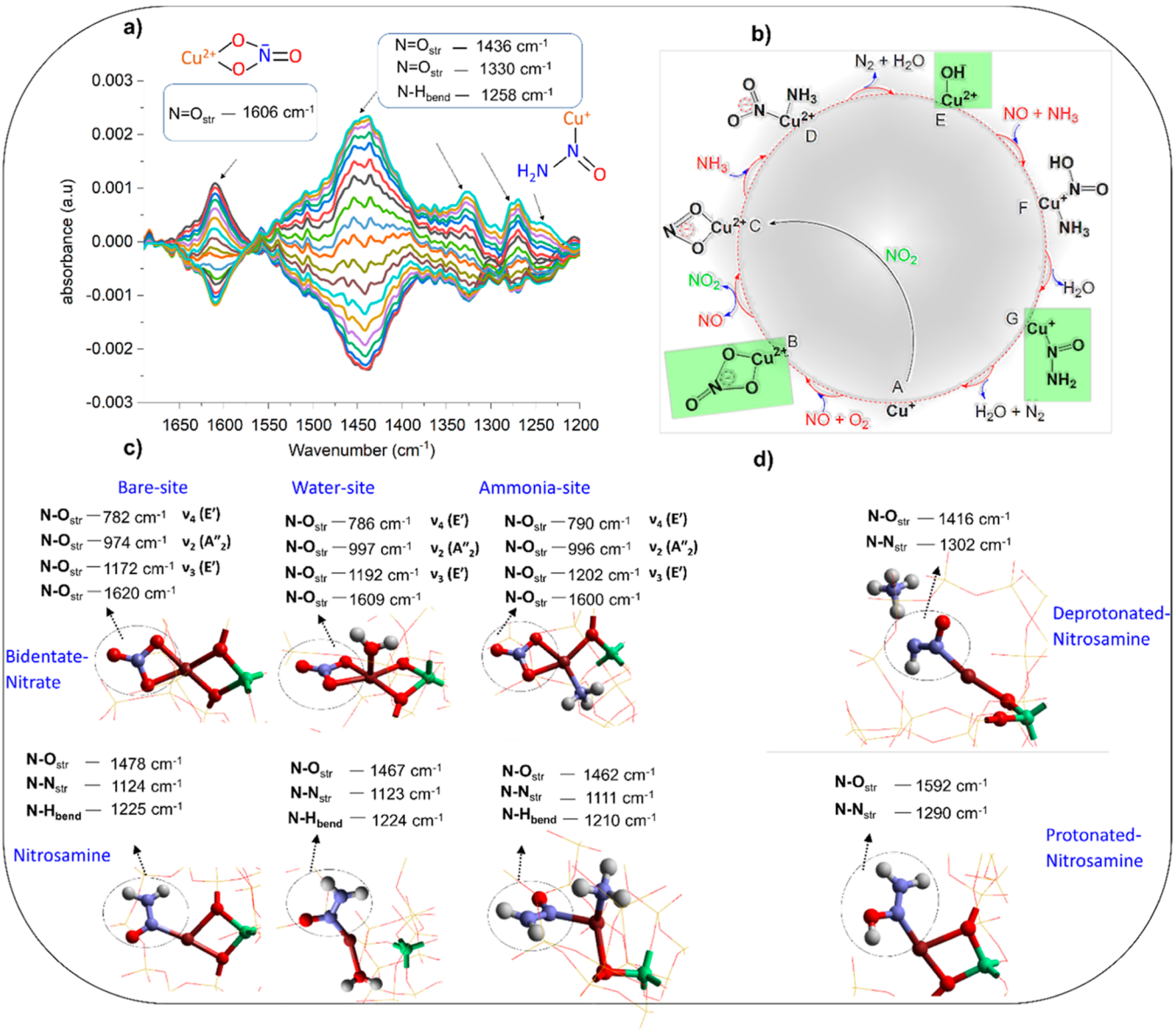

Figure 3. Spectroscopic signatures: (a) concentration modulation ME DRIFTS experiment with the corresponding phase-resolved spectrum, (b) reaction cycle highlighting the identified species, (c) data obtained from QM/MM calculations for bidentate Cu nitrate (Cu−NO_3) and Cu-nitrosamine (Cu−N(=O)−NH_2) species for the neutral system, and (d) for the deprotonated and protonated system. Color codes: Cu (brown), Al (green), O (red), N (blue), and H (white). The framework SiO_2 is shown using a wire framework motif.

scanner velocity (0.9 s per spectrum) and at 4 cm^{-1} resolution. Solenoid valves were used to repeatedly switch between gases during a concentration modulation excitation experiment which was functioned using OPUS software (Bruker).

3. RESULTS AND DISCUSSION

An NH_3-SCR reaction mechanism has been proposed by Janssens *et al.*, who show both standard and fast NH_3-SCR of NOx in a complete cycle that can produce the correct stoichiometry for the reaction.[32] In contrast, in our study, the focus is on solvent effects on the reactivity of the Cu-CHA, and, as argued, it provides key insights into the reaction mechanism from accurate hybrid-QM/MM calculations and concentration modulation ME DRIFTS experiments. Hybrid-QM/MM investigations, DRIFTS experiment, and in-depth scrutiny of solvent effects allowed us to explore especially the intermediate−solvent interactions and identify the important species participating in the NH_3-SCR event both on the bare and on the solvated sites. The computational mechanistic study focuses on these results, which complement and give insight into the experimental findings.

3.1. Vibrational Study. First, we performed DRIFTS experiments exploiting (concentration) modulation excitation spectroscopy (MES) and phase-sensitive detection (PSD) to determine the evolution of species in response to a stimulus; in this case, the NO flow during a constant stream of 500 ppm NH_3 and 10,000 ppm O_2 produces N_2 akin to the standard NH_3-SCR reaction at 250 °C.[38] This approach allows us to observe the formation and consumption of short-lived intermediates in the catalytic reaction, crucially, the detection of species, which had not been previously observed experimentally. The data are shown in Figure 3a.[38] Notable observations included the initial consumption of $[Cu^{2+}(OH)]^-$ to form an important intermediate, which has been identified

https://doi.org/10.1021/jacs.2c09823
J. Am. Chem. Soc. 2023, 145, 247−259

as copper nitrosamine (Cu−N(=O)−NH_2) based on the observation of evolving bands in the IR spectrum at 1436 cm^{-1} (N=O_{str}), 1330 cm^{-1} (N=O_{str}), and 1258 cm^{-1} (N−H_{bend}). Below 1200 cm^{-1}, we are unable to collect reliable spectroscopic data due to the overlapping of zeolite framework vibrations with other bands. The next species detected in the cycle was a bidentate nitrate (N=O_{str} at 1606 cm^{-1}). Note that all bands appear with a different "phase", or time during the experiment, indicating that the corresponding species are not typically present at the same time. Furthermore, Figure S5 shows the 2400 DRIFTS spectrum collected throughout the course of the modulation experiment in which NO is turned "on/off" repeatedly between 0 and 500 ppm, while the concentration of other reactive components, NH_3 and O_2, remains constant. Note that no discernible changes can be detected since the continuous presence of NH_3 and products of the reaction (H_2O) dominate the spectrum, particularly in the region between 2500 and 3500 cm^{-1}.

Second, we calculated the harmonic vibrational spectra of selected intermediates. The harmonic values obtained were scaled using vibrational scaling factors (see Supporting Information), which were determined by comparing experimental and computational harmonic values using a representative set of gas-phase molecules. We focused on bands of nitrosamine (N−O_{str} and N−N_{str}) and nitrate (N−O_{str}); the yielded scaling factor to calculate the vibrational frequency of N−O_{str} of nitrosamine is 0.915, while for the N−N_{str}, it is 0.918. Similarly, the corresponding scaling factor we applied for the N−O_{str} of nitrate is 0.943.

As shown in Figure 3b, for the bare Cu-nitrosamine (Cu−N(=O)−NH_2) (species G, Figure 3b) species, we found a vibrational stretching band around 1478 cm^{-1} compared to our experimental value of 1436 cm^{-1}, tentatively ascribed to the N=O_{str} mode. Haszeldine and Jander reported the N=O_{str} band at 1488 cm^{-1} which is close to our calculated frequency.[39] Also, bands in the region 1408−1486 cm^{-1} have been reported by Piskorz and Urbanski[40] and Tarte[41] and assigned to the N=O_{str} frequency of nonassociated dialkylnitrosamine (in nonpolar solvent: CCl_4). They also reported peaks for N=O_{str} between 1346−1265 and 1321−1292 cm^{-1}, which can be broad and strong or of medium strength. Importantly, this can be also seen in our measured DRIFTS spectra [(N=O_{str}), 1330 cm^{-1}]. Furthermore, Kedrova *et al.* have observed the vibrational frequencies of associated nitrosamine and identified both N=O_{str} (1470−1495 cm^{-1}) and N−N_{str} (1055−1060 cm^{-1}) bands.[42] On physisorption of water and ammonia at Cu sites, we observed the N-O_{str} band shift down to 1467 and 1462 cm^{-1}, respectively. The lower frequency spectral features found in our QM/MM calculations are, in particular, due to N−N stretching vibrations of Cu-nitrosamine (Cu−N(=O)−NH_2) species. For the bare site, the N−N stretching frequency is calculated as 1124 cm^{-1} as compared to the reported experimental values in the nitrosodimethylamine (1052 cm^{-1}) and di-*N*-nitroso-pentamethylenetetramine (1106 cm^{-1}).[40] For the water- and ammonia-solvated sites, the N−N_{str} is found at 1123 and 1111 cm^{-1}, respectively. In addition to the N=O_{str} and N−N_{str} bands for nitrosamine species, we also examined the N−H bend, which is likely to appear in this region; the computed value for the bare site is at 1225 cm^{-1}, whereas for the water- and ammonia-solvated sites, it is found at 1224 and 1210 cm^{-1}, respectively. The reduction of the vibrational frequency of these modes shows the ligand effect as stronger ligands may weaken the bonding.

Next, we investigated a bidentate nitrate species (species B, Figure 3b) with a focus on the N=O_{str} stretching mode. Generally, nitrate species have four notable modes.[43,44] Our calculations show that the bare bidentate Cu−NO_3 structure possesses the main N=O_{str} stretching frequency of 1620 cm^{-1}, while for the physisorbed water and ammonia, it is found at 1609 and 1600 cm^{-1}, respectively. All these three bands are quite close to our experimental DRIFTS value of 1606 cm^{-1} and to earlier reports[45,46] of the nitrate N=O_{str} difference FTIR band in Cu-SSZ-13. In addition, small broad bands that appeared in our experimental findings in the region of 1230−1250 cm^{-1} could be assigned to the antisymmetric stretch (ν_3 (E′)) of the N−O band, as reported by Zapata and Garcia-Ruiz.[43] However, our QM/MM calculation shows this band at relatively lower frequencies for this mode; for instance, it is seen at 1172 cm^{-1} for the bare site, while for physisorbed water and ammonia sites, it appears at 1192 cm^{-1} and 1202 cm^{-1}, respectively. Finally, two bands that originated by out-of-plane and in-plane deformation modes for nitrate species are displayed. The out-of-plane deformation band (ν_2 (A_2'')) is normally located within the range of 800−900 cm^{-1}, while the in-plane band (ν_4 (E′)) ranges from 700 to 780 cm^{-1} in nitrate salts.[43,44] Our calculated out-of-plane deformation occurs at a somewhat higher frequency, as seen in Figure 3b; however, the in-plane deformation has appeared almost in the same region as previously reported.[43]

One of the significant effects of solvation is the possibility of site deprotonation due to a proton transfer to solvents even if only as a transient species. Therefore, we completed this analysis by studying vibrations of a negatively charged intermediate species that would result from such deprotonation by possibly abstracting the proton from the −NH_2 group of nitrosamine to form NH_4^+ ions (see Figure 3d). The calculated N−O_{str} (1416 cm^{-1}) band is found at somewhat lower frequencies for the deprotonated nitrosamine NH_4^+(Cu−N(=O)−NH) species compared to the neutral system (1478 cm^{-1}), while the N−N_{str} stretching bands for this species appear at a relatively higher frequency of 1308 cm^{-1} than the neutral system (1124 cm^{-1}). There is a mixed asymmetric stretch mode of the NH_4^+ group combined with N−N_{str}, which may be the reason that N−N_{str} appears at a higher frequency than expected.

Inversely to the deprotonation of nitrosamine species, we also examined the likely protonation of Cu-nitrosamine (Cu−N(=O)−NH_2) that generates an −OH site, that is, (Cu−N(=OH)−NH_2). The calculated N−O_{str} band (1592 cm^{-1}) in this case was found at significantly higher frequencies compared to both deprotonated nitrosamine (1416 cm^{-1}) and neutral system (1478 cm^{-1}). Based on the result obtained, we infer that the experimental DRIFTS data show either neutral or deprotonated nitrosamine rather than protonated species. Moreover, we also carried out a separate vibrational analysis on Cu−(N(=O)−OH)−NH_3 (species F, Figure 3b), a postulated species which further decomposes to the (Cu−N(=O)−NH_2) species. The N−O_{str} band appeared for this intermediate at 1585 cm^{-1} (Figure S2).

Furthermore, we examine the N=O_{str} vibrational mode of bidentate-nitrite (Cu−NO_2) (species C, Figures 3b, S3) to determine whether the 1606 cm^{-1} band in the DRIFTS spectrum originates from the nitrate or nitrite. The computed N=O_{str} band of this particular species is, however, found to be

https://doi.org/10.1021/jacs.2c09823
J. Am. Chem. Soc. 2023, 145, 247−259

Table 1. Features Observed in a Concentration ME DRIFTS Experiment's Time-Resolved Spectrum under SCR Conditions (NO Gas Switch Pulse Sequence)[a]

DRIFTS (cm^{-1})	vibrational mode	strength	width	calculated IR mode[b]	ref
1606	N=O stretch (nitrate)	medium	sharp	1600 (B), 1609 (H), 1620 (N)	45, 46
1436	N=O stretch (nitrosamine)	strong	sharp	1478 (B), 1467 (H), 1462 (N)	39−42
1330	N=O stretch (nitrosamine)	small	medium		41
1258	N−H bend (nitrosamine)	small	sharp	1225 (B), 1224 (H), 1210 (N)	
1230−1250	N−O*anti*-symm. stretch (nitrate)	small	broad	1172 (B), 1192 (H), 1202 (N)	43, 44
1210	N−N stretch	small	medium	1124 (B), 1123 (H), 1111 (N)	40, 42

[a]Assignment is based on an analysis of the literature and calculated vibrational spectra of reactant intermediates shown in Figure 3b. [b]B, bare; H, physisorbed H_2O; and N, physisorbed NH_3.

significantly lower than the $N{=}O_{str}$ band of the bidentate-nitrate species at 1273 cm^{-1}, while for the solvated H_2O and NH_3 active sites, it is observed at 1263 and 1260 cm^{-1}, respectively. Notably, the calculated bands are comparable with the experimental values of *ca.* 1229 cm^{-1} for the isostructural linear nitrite species reported in refs 47 and 48.

We have performed a similar calculation on (Cu−(NO_2)−NH_3) (species D, Figures 3b and S4); however, again we found that the NO band for this species is lower than the 1606 cm^{-1} band in the DRIFTS spectrum assigned to $N{=}O_{str}$ vibration for all three sites. Based on the calculated vibrational modes, we infer that the spectroscopic signatures that appear in the DRIFTS spectrum can be tentatively assigned to the nitrate and nitrosamine species. Furthermore, we do not detect the N−O signatures in the DRIFTS spectrum for the nitrite (species C) and the species D and F in the cycle and even the first Cu−NO(OH) interactions on NO adsorption, indicating that these species are too short-lived to be observed experimentally. Hence, we propose the assignment of the DRIFTS spectral features summarized in Table 1 and shown in Figure 3a.

Furthermore, we examine the O−H and $N{-}H_{str}$ vibrational features for the competing $[Cu^{2+}(OH)]^+$ and Brønsted acid sites under an NH_3-SCR environment. In the DRIFTS spectrum (Figure S5), there are multiple vibrational bands in the region between 2500 and 3500 cm^{-1} as the spectrum is mostly dominated by NH_3 and H_2O. The most notable feature in the phase-resolved spectrum is, however, that at 3655 cm^{-1}, which is indicative of $[Cu^{2+}(OH)]^+$ species that exhibit a greater fluctuation than those related to silanol groups or bridging hydroxyls, which is also reported by Giordanino *et al.*[49] Our calculated value (3668 cm^{-1}) is in good accordance with the DRIFTS experimental value and with the reported data.[45] The experimental attribution of this band to a $[Cu^{2+}(OH)]^+$ species was based on its response to changes in gas composition, indicating that this species actively participates in the catalytic mechanism.[38] The vibrational signatures of the likely NH_3 adsorption on the Cu^{2+} active sites are also confirmed by theory and experiment. In the corresponding DRIFTS spectrum, the N−H band which appears at 3332 cm^{-1} is in good accordance with the computed value of 3336 cm^{-1}. Moreover, we detect the N−H bending features at 1620 cm^{-1} in the DRIFTS spectrum which is reproduced in our calculations with an accuracy better than 1 cm^{-1} and agrees well with previous work.[50] To study the competitive reaction pathway between NH_3 adsorbed on Cu sites and Brønsted sites, we analyzed the vibrational signatures of the NH_3 adsorption on the Brønsted acid site, the interaction which may lead to evolution of NH_4^+ ions owing to the NH_3 protonation over these acid sites. The band intensity grows from *ca.* 1454 cm^{-1} in the DRIFTS spectrum (see Figure S5), indicating the consumption of the ν(O−H) band associated with the Brønsted acid sites. The position of this band is confirmed by our computed value of 1455 cm^{-1} and previous work[49] for NH_4^+ ions. The N−H stretching band of NH_4^+ ions appears at 3272 cm^{-1} in the DRIFTS spectrum, which also agrees with the calculated vibrational value at 3278 cm^{-1}.

Our computational analysis provides a clear assignment (Table 2) of all main spectroscopic features of the species presented in Figure 3b.

Table 2. Calculated Vibrational Bands of Key Intermediate Species Presented in the NH_3-SCR Catalytic Cycle—See Figure 3b

species	wavelength (cm^{-1})[a]	description of IR active mode
Cu−NO_3 (species B)	1600 (B), 1609 (H), 1620 (N)	N=O stretch
Cu−NO_2 (species C)	1273 (B), 1263 (H), 1260 (N)	N=O stretch
(Cu−(NO_2)−NH_3) (species D)	1501 (B), 1481 (H), 1464 (N)	N=O stretch
	3445 (B), 3450 (H), 3447 (N)	N−H stretch
Cu−(N(=O)−OH)−NH_3 (species F)	1585 (B), 1579 (H), 1575 (N)	N=O stretch
	3313 (B), 3471 (H), 3485 (N)	N−H stretch
	3197 (B), 3216 (H), 3226 (N)	O−H stretch
(Cu−N(=O)−NH_2) (species G)	1478 (B), 1467 (H), 1462 (N)	N=O stretch
	3482 (B), 3493 (H), 3517 (N)	N−H stretch
$[Cu^{2+}(OH)]^+$ adsorbed NH_3	3336	N−H stretch
	3668	O−H stretch
	1620	N−H bend
Brønsted acid site adsorbed NH_3	3279	N−H stretch
	1455	N−H bend

[a]B, bare; H, physisorbed H_2O; and N, physisorbed NH_3.

3.2. Comparison of Reaction Energetics with Experiment. Next, we assess our computational approach for the overall de-NOx reaction energy that involves NO activation to stable long-lived intermediates and products. To this end, we compare the simulated data with experimental measurements and analyze the results obtained (Tables S3 and S4). First, we calculated the reaction energy for eq 2, an NO-activation pathway using computational parameters described in Section 2.1 (B97-2[31] functional and the def2-TZVP[30] basis set). The

https://doi.org/10.1021/jacs.2c09823
J. Am. Chem. Soc. 2023, 145, 247−259

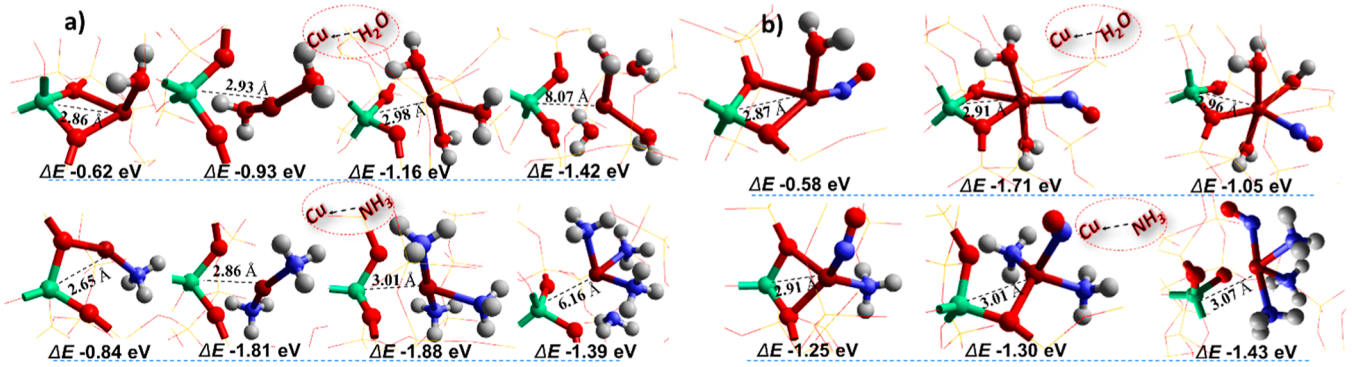

Figure 4. Interaction of physisorbed (a) water and ammonia with Cu(I)-CHA active sites, and (b) behavior of NO on solvated Cu(I)-CHA site. The model used is shown as an extra framework. Color codes: Cu (brown), Al (green), O (red), N (blue), and H (white).

overall experimental $\Delta_f H_0^\circ$ value is −9.01 eV (−869 kJ/mol), which is calculated from the standard enthalpy of formation (Table S5) of the gaseous species involved in this reaction. The calculated theoretical value is −8.37 eV, which is similar to the previous calculations (∼−8.45 eV, estimated from Figure 3 of ref 32). Thus although the two theoretical estimates are within 0.08 eV of each other, there remains a small but significant deviation from the experimental value.

3.3. Cu Displacement on Solvation. The promoting effect of water on the migration of Cu species suggested that unanchored Cu ions migrate to form active sites which can promote the SCR reaction.[18] In our calculations summarized in Figure 4a, we observed that an increase in water coordination to the Cu-active sites displaces the Cu species away from the CHA framework. As the number of H_2O molecules around the Cu(I)-CHA increases, the interaction between the framework and Cu species becomes weaker. In the case of four H_2O molecules, the distance between Al and Cu is calculated to be 8.07 Å, consistent with the understanding that water molecules promote the mobility of Cu ions. Similarly, the effect of NH_3 solvation during the oxidation part of the SCR reaction is crucial. Some previous reports suggest that the NH_3-solvated Cu(I) sites interact weakly with the zeolite framework and move away as a mobile species to react with the O_2 and yield an O-bridged Cu(II) dimer;[51] we find an increase in bond length between Al and Cu as the number of NH_3 molecules increases, suggesting that an enhanced number of NH_3 molecules can detach Cu species from the framework. *Ab initio* molecular dynamics (AIMD) simulations show that after the adsorption of one NH_3 molecule in Cu-SAPO-34[52] at 298 K, the Cu^+ cation is somewhat displaced yet remains coordinated with one of the framework oxygens in an $H_3N-Cu-O$ bond, which is also evident from experiments on Cu-SSZ-13.[49] These studies demonstrate that the Cu−O bond in the Cu^+-NH_3 system is broken by the adsorption of a second NH_3 molecule, resulting in the formation of a linear $Cu^+(NH_3)_2$ complex that can move readily inside the pore. Our QM/MM simulations agree with these findings, as can be observed from Figure 4a. Furthermore, Paolucci *et al.*[10] used *ab initio* metadynamics and a supercell with a minimum image distance in excess of 10 Å to evaluate the mobility of $Cu^I(NH_3)_2$ complexes over time scales which are inaccessible to conventional AIMD. Their results supported by experimental observations show a ∼9 Å diffusion length for a Cu ion that penetrates an 8-MR window separating two adjacent CHA cages. In our study, we employed a more detailed model of the solvent behavior in the Cu-SSZ-13 system. Similar to the abovementioned study, we start our analysis with a single-solvent adsorbate molecule simulating both water and ammonia. Next, we introduced stepwise a series of solvent molecules bringing the solvent content to four molecules per cage. Upon adsorption, we observed a pronounced displacement of the Cu ion away from the framework Al site. In the case of water, the calculated distance between Al and Cu is 8.07 Å, while for the solvated Cu−NH_3 case, it is 6.16 Å, consistent with the understanding that solvent molecules promote the mobility of Cu ions. In contrast to the report by Paolucci *et al.*,[10] we do not observe the penetration through the 8-MR window, which could be attributed to the different boundary conditions in our simulations. Notably, the Cu ions in our study are not forced to move away from the Al site but displace spontaneously as a result of geometry optimization from their initial position close to the Al site in response to the strong interaction of the polar solvent with both framework and extraframework metal cations.

We also examined the approach of NO toward the solvated Cu(I)-CHA and infer that in the presence of water, the effect of NO is vital, as it restricts, to some extent, the displacement of the Cu-ion species from the framework (Figure 4b). This is apparent from the corresponding separation distances (2.96 Å) between Cu and Al when compared with those when NO is not present, which can prevent Cu(II) dimer formation and promotes the formation of nitrate species.[53,54] In addition, it also suggests that the presence of NO might prevent the mobility of Cu ions in the presence of water. We, however, observed a complete detachment of Cu ions from the framework when NO interacts with three NH_3 coordinated sites with a distance of 3.071 Å between Cu and Al (Figure 4b).

3.4. Adsorption Study. We examine first the binding energies of the gaseous reactant molecules both on the Cu(I)-CHA and Cu(II)-CHA sites.

From the results reported in Figure 5, considering the behavior on the Cu(I) site, we note that the adsorption of NO, NH_3, and H_2O on the Cu^+-/CHA site is, as expected, exothermic. The binding energy for NH_3, yielding NH_3-Cu^+, is calculated as −0.84 eV (−81 kJ/mol)[32,55] where the reported average experimental heat of adsorption for ammonia on Cu-Beta[56] and Cu-CHA[57] is nearly −100 kJ/mol. The experimental values, however, should be treated with caution as Cu-exchanged zeolites would still have a significant fraction of strongly adsorbing Brønsted acid sites.[58,59] We have also examined the interaction of ammonia with the Brønsted acid

https://doi.org/10.1021/jacs.2c09823
J. Am. Chem. Soc. 2023, 145, 247−259

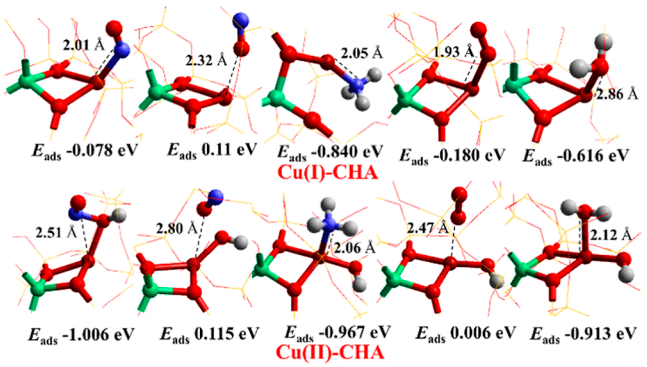

Figure 5. Reaction adsorption energies of NH_3, NO (with both the O- and N-end down), H_2O, and O_2 on Cu(I)-CHA and Cu(II)−OH/CHA sites. The model used is shown as an extra framework. Color codes: Cu (brown), Al (green), O (red), N (blue), and H (white). The framework SiO_2 is shown using a wire framework motif.

site and found a binding energy of −1.1 eV (−106 kJ/mol), which is appreciably higher than that of the Cu Lewis site and is close to the experimental report. The heat of NH_3 adsorption over non-exchanged zeolites H-CHA has been reported to be as high as −145 kJ/mol (obtained using microcalorimetry techniques),[60] which is appreciably stronger and could be related to the Brønsted acid complexes, which warrants a separate investigation.

Furthermore, the reported studies also suggest that the heat of adsorption decreases with increased ammonia coverage.[57] It is reported that the binding of NH_3 on Cu^+ strongly influences the interaction of Cu with the framework of CHA; however, depending on the number of NH_3 molecules bound and temperature, cation mobility can become possible.[52] In this context, we observed that a single physisorbed NH_3 molecule detaches Cu^+ from one of the framework O atoms, making a new coordination adduct, $H_3N{-}Cu{-}O$, with a distance between Al and Cu of 2.645 Å. H_2O also exothermically binds to the Cu(I)-CHA sites with a binding energy of −0.62 eV (−59 kJ/mol), but the monovalent Cu remains attached to the two framework O atoms. Furthermore, Lercher and co-workers employed a periodic PBE + D3 approach and obtained an adsorption energy of −77 kJ/mol for water on the Brønsted acid site of H-MFI,[61] whereas a value of −78 kJ/mol is obtained for the H-CHA by a hybrid MP2/PBE calculation.[62] We also observed that NO weakly adsorbs on bare Cu(I)-/CHA, through the N atom (with a binding energy of only −0.08 eV); however, it is more favorable on solvated ammonia Cu(I) (−1.25 eV) and water Cu(I) (−0.58 eV) sites, where the corresponding experimental heat of adsorption is −65 kJ/mol (−0.70 eV) on Cu-Beta.[56]

Turning now to the Cu(II) sites, NH_3 and NO interact favorably with divalent Cu (II)−OH sites. NO binds through the O atom (−OH) (−1.01 eV), suggesting that it preferentially binds to the OH site of Cu(II)−OH, generating an HONO species. The formation of the HONO species has been described earlier.[47,63] In the case of NH_3, strong bonding to the Cu(II) site is calculated, with a binding energy of −0.97 eV (−93 kJ/mol), and as seen in Figure 5, the attachment of

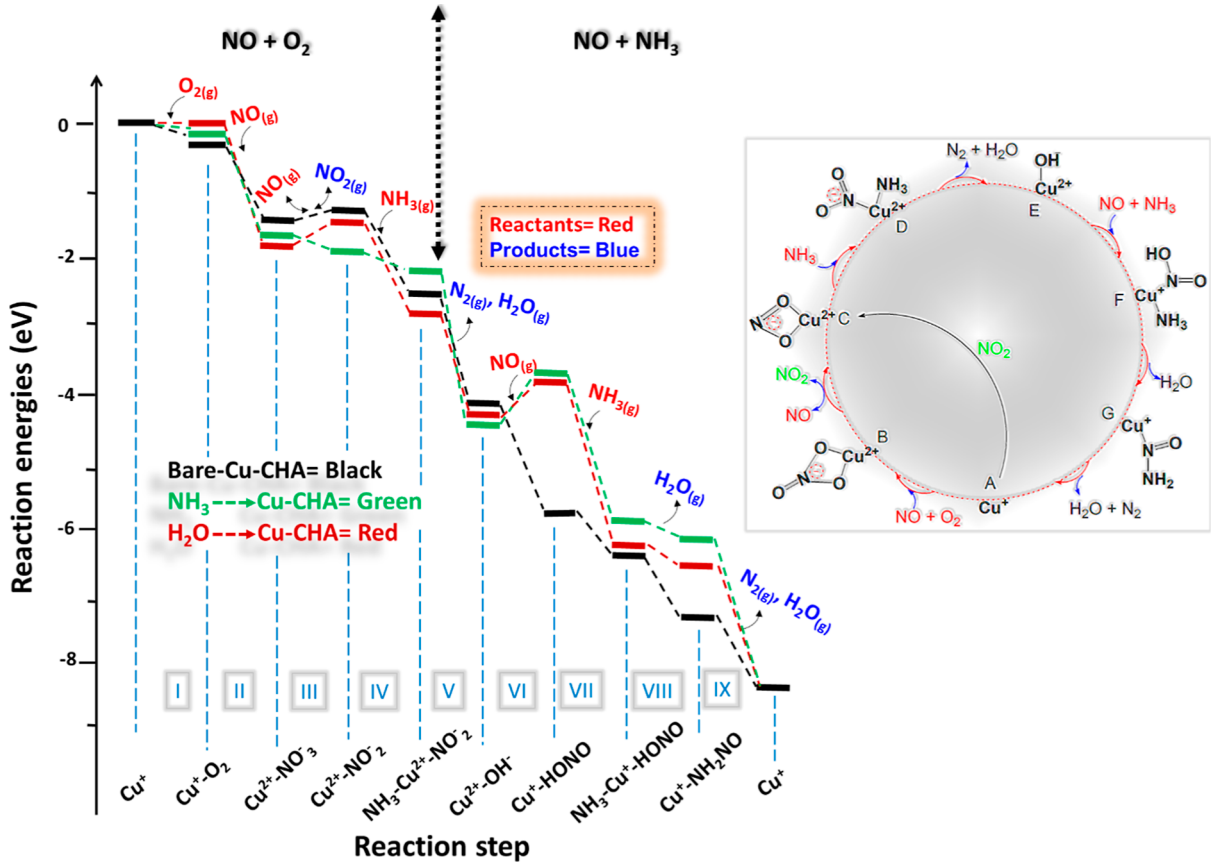

Figure 6. Potential reaction-energy landscape for NH_3-SCR on the activated Cu-CHA site and (black) on the bare site, (green) with physisorbed ammonia and (red) with physisorbed water. Inset right: NO-activated NH_3-SCR of the NOx catalytic cycle.

https://doi.org/10.1021/jacs.2c09823
J. Am. Chem. Soc. 2023, 145, 247−259

Cu(II) with the framework O is intact. We also demonstrate that water can interact strongly with the divalent Cu site (with a binding energy of −0.91 eV), suggesting that water can affect the reactivity of active sites.

Based on the interaction of molecules with the active sites, we conclude that the adsorption of NO species with the O-end down is uncompetitive (with a positive energy) on both Cu^+ (0.11 eV) and Cu^{2+} (0.12 eV) sites, suggesting that the N-end down is the only feasible attachment to Cu-CHA sites. We found that O_2 preferably binds to Cu(I) sites with a binding energy of −0.18 eV (−17 kJ/mol) as reported before, while on the Cu^{2+}−OH^-/CHA site, the adsorption energy is calculated to be positive (0.01 eV),[52] which rules out the possibility of O_2 binding to the Cu^{2+}−OH^-/CHA, hence, signifying that O_2 plays a key role in the reoxidation of the Cu^+-site.

3.5. Catalytic Cycle. During the NH_3-SCR cycle, molecules including NO, NH_3, O_2, N_2, and H_2O are either adsorbed or desorbed from the Cu-CHA site, and the intermediate species are generated at each step (Figure 6). The adsorption of NO and O_2 on Cu^+-/CHA generates nitrate and nitrite species which undergo decomposition to N_2 and H_2O; this half cycle of the NH_3-SCR is, as noted, known as the oxidation part, which is followed by the reduction of Cu^{2+} where Cu^{2+}−OH^-/CHA reacts with both NO and NH_3, with Cu^{2+} reduced to Cu^+ while generating N_2 and H_2O as a product, as is evident from both experimental and theoretical studies.[52] The calculated adsorption energies of the corresponding gaseous species allow us to obtain the reaction energy landscape. Note that in the DRIFTS spectra, all bands appear with a different "phase" or time during the experiment, indicating that the corresponding species are not typically present at the same time and giving further credence to the cyclical nature of the proposed mechanism shown in the inset of Figure 6.

Considering the NH_3-SCR of the NOx cycle, first, without physisorbed solvent molecules, the corresponding reaction energy landscape is shown in Figures 6 (black lines) and S7. The starting point for the chemical reaction is an isolated Cu(I) site that activates the O_2 molecule (step I). The energy diagram demonstrates that O_2 adsorption is exothermic (−0.18 eV) over the Cu(I)-CHA site which is followed by NO adsorption that generates the Cu−NO_3 species with a formation energy of −1.34 eV while simultaneously oxidizing Cu(I) to Cu(II) (step II). It is evident from previous reports that gaseous NO_2 can react with the Cu^+ site, yielding a bidentate Cu nitrite species (step III), which is often considered the fast-SCR reaction.[64] The reaction of gaseous NO with nitrate[54] is reported to be a two-step process where first NO coordinates with the nitrate species and then decomposes to nitrite with the release of gaseous NO_2. To this end, we found a total energy change of +0.17 eV from the nitrate to nitrite step. In the case of the NH_3 reaction with the nitrite species, an intermediate (step IV) is formed with a formation energy of −1.24 eV. Furthermore, we found that NH_3 can also react with the Cu−HONO site that generates an NH_3−Cu−HONO intermediate (step VII) with an H_3N−Cu bond length of 2.160 Å and a formation energy of −0.63 eV. Subsequently, it decomposes and leads to the generation of an important intermediate, the Cu-nitrosamine (Cu−N(=O)−NH_2) (step VIII), which is considered to play a key role in the NH_3-SCR reaction as it involves the formation of the first N−N bond in the N_2 product. The QM/MM results agree with the sequence of species identified in our DRIFTS data. The existence of both nitrosamine and nitrate in the DRIFTS spectra is also evident from the calculated QM/MM harmonic vibrational data.

3.5.1. Effect of Water Solvation. Water is one of the main products of NH_3-SCR reaction, and therefore, the hydrated state of the active sites cannot be ignored.[65] Taking into account the calculated adsorption energies of H_2O on Cu(I)-CHA (−0.62 eV) and Cu(II)-CHA (−0.91 eV) sites, we suggest that the NH_3-SCR reaction proceeds differently on solvated Cu-CHA sites. Using the same computational approach, we have studied the effect of water on the formation of the intermediate species; single water molecules are attached to the isolated Cu(I)/Cu(II) active sites to which intermediate species are bound. The corresponding reaction energy landscape is shown in Figures 6 (red lines) and S8. We observe notable differences in the formation energies of some important steps. For example, our results show that without physisorbed water, the formation of nitrate species is less favorable (−1.34 eV) than in the presence of water (−1.69 eV) (step II), suggesting that water can promote the re-oxidation half-cycle, which is also supported by experimental findings as reported by Wan *et al.*,[18] showing that water could markedly enhance NO reduction. In contrast, we found that on the water-occupied −Cu-CHA site, the formation of Cu-nitrosamine (Cu−N(=O)−NH_2) (step VIII) is less favorable (−0.11 eV) than in the absence of water (−0.66 eV), suggesting that water can slow down the formation of this species, which can ultimately affect the reduction part of the NH_3-SCR cycle. We observe that the effect of water on nitrosamine is more significant (+0.55 eV) than on the nitrate (−0.35 eV), which implies that the impact of water could be a (slight) net negative influence on activity. Commensurate with this, it has also been reported previously that residual H_2O or hydrocarbons can block the active sites or alter their activity.[66]

3.5.2. Effect of Ammonia Solvation. Previous experimental evidence showed that preadsorbed NH_3 at 300 or 250 °C can enhance NOx reduction; however, low activity of NO reduction was observed below 150 °C.[14] From the calculated binding energies of NH_3 for both Cu(I)-CHA (−0.62 eV) and Cu(II)-CHA (−0.91 eV) sites, we can infer that the reactive sites occupied by NH_3 molecules can influence the mechanism. We have investigated the influence of ammonia on the formation of the intermediate species, as shown in green lines in the energy profile (Figures 6 and S9). Notably, the formation of Cu bidentate nitrate species (Cu−NO_3) on the physisorbed NH_3 site is found to be more favorable (−1.59 eV) than with the bare site (−1.34 eV) (step II). In the case of physisorbed water and the bare site, the generation of nitrite under the release of NO_2 is found to be endothermic, but for physisorbed ammonia, it is exothermic (step III). In addition, the formation of the important intermediate, Cu-nitrosamine (Cu−N(=O)−NH_2) (step VIII), is less favorable on the physisorbed ammonia active sites (−0.31 eV), when compared to the bare site (−0.66 eV), indicating that physisorbed ammonia can block the active sites for the NH_3 + NO activation half cycle.

3.6. H_2NNO Decomposition. An important step in the NH_3-SCR mechanism is the reaction of NH_3 with HONO that generates the NH_3−Cu−HONO intermediate which eventually leads to the formation of the key intermediate Cu-nitrosamine (Cu−N(=O)−NH_2), as shown in Figure 6 (step VIII). The decomposition of H_2NNO has been extensively studied and proceeds through the transformation of several

https://doi.org/10.1021/jacs.2c09823
J. Am. Chem. Soc. 2023, 145, 247−259

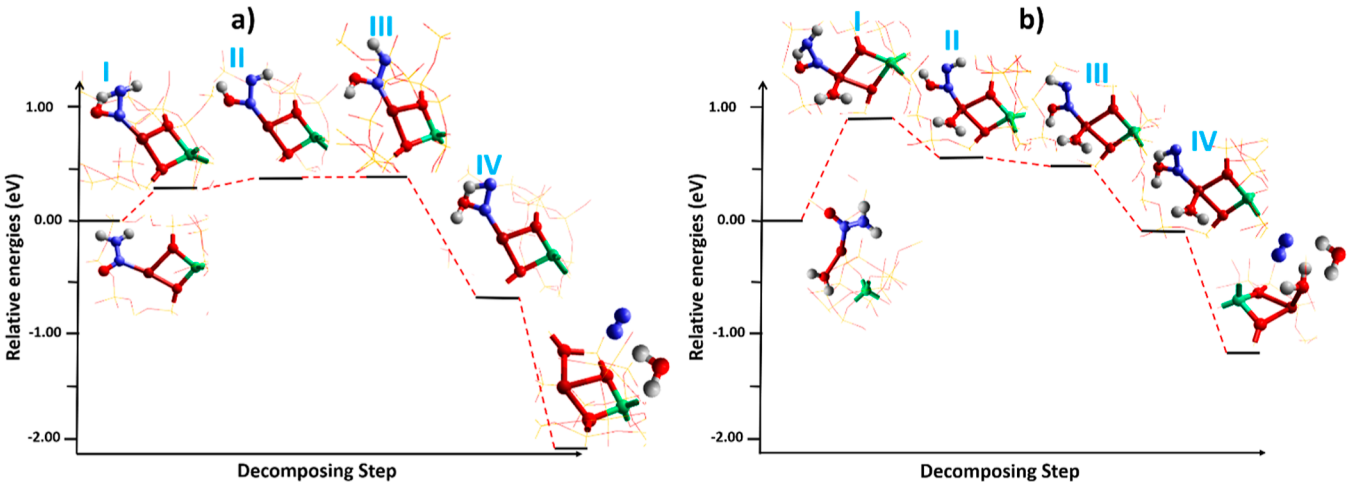

Figure 7. Calculated potential energy surfaces for H_2NNO isomerization (a) without water and (b) in the presence of physisorbed water on the Cu-CHA-sites. The model used is shown as an extra framework. Color codes: Cu (brown), Al (green), O (red), N (blue), and H (white).

important isomers with high activation barriers.[67−69] For example, DFT calculations showed that the energy barrier for the H_2NNO decomposition is considerably lowered *via* proton exchange between the Brønsted acid site and H_2NNO over V_2O_5,[70] the mechanism of which is similar to dehydrogenation of propane over vanadia.[71] A similar study has been conducted over Cu-CHA where the decomposition of H_2NNO is investigated on Brønsted acid sites.[72] Such a study has also been reported over Cu-SAPO-34[73] and ZSM-5[74,75] using a cluster-based computational approach. As it is found that the solvent can coordinate to the Cu-site, we, therefore, investigated the decomposition pathway of H_2NNO on isolated Cu-CHA active sites both in the presence and absence of physisorbed water (Figure 7). The schematic illustrations of isomeric decompositions of H_2NNO intermediates are shown in Figure S10. The adduct rearrangement process of H_2NNO species starts with 1,3 H-transfer, breaking one N−H bond with the transmission of an H to an adjacent O atom, which leads to the formation of an O−H bond. The H-transfer leads to two isomers *cis*−*trans* (II) and *trans*−*cis* (III) through the four-membered ring(I). The total energy change from structures (I) to (II) and (III) are calculated as 0.04 and 0.06 eV on the bare site, respectively, while with ligated water, it is −0.33 and −0.46 eV, respectively, suggesting some positive impact of solvated sites on the energetics of this step. From H_2NNO to HNNOH, the H-transfer is accompanied by shortening of the N−N bond (from 1.35 to 1.299 Å) with lengthening of the N−O bond (from 1.208 to 1.306 Å) that eventually ends with the termination of respective bonds and generation of H_2O and N_2 as products. We have noted that the increased coordination of H_2O molecules detached Cu−H_2NNO from the framework (Figure S11), showing that the solvent can affect the binding of Cu−H_2NNO species to the framework.

3.7. Reactivity of HONO. We also examined the reactivity of Cu−HONO species for NH_3, H_2O, O_2, and NO, which are the key reactants and products in the NH_3-SCR reaction. We have found that NO can bind with the Cu(II)−(OH) site forming the Cu−HONO species[20,53,76] that can react with NH_3 to yield NH_4NO_2, a short-lived and unstable species which can decompose to N_2 and H_2O. The subsequent desorption of HONO is endothermic (energy barrier: 0.145 eV) as previously reported;[76] we, therefore, performed a series of calculations to assess the interaction of other species with the Cu−HONO site, as displayed in Figure S12. Considering the approach of solvent molecules first, we found that the interaction of Cu−HONO with H_2O is exothermic, while with ammonia, it is endothermic. The binding energy of H_2O is calculated to be −0.39 eV with a bond distance between O and Cu of 2.155 Å. In the case of NH_3, the binding energy is 0.99 eV with a bond distance between N and Cu of 2.160 Å. The interaction of dioxygen with the Cu−HONO site is in the superoxo (O^{2-}) mode with an average bond distance of 2.127 Å between O and Cu. We also note the interaction of NO with Cu−HONO, forming a NO−Cu−HONO adduct.

4. SUMMARY AND CONCLUSIONS

The present study has aimed to confirm the identity of key intermediates in the NH_3-SCR reaction and elucidate the role of physisorbed solvents, as the Cu-CHA active sites will be affected by solvent molecules. The main catalytically active sites that facilitate the adsorption of species are both monovalent- and divalent-copper sites that can drive the NH_3-SCR to generate important intermediate species including nitrates and nitrites. By understanding the parallels between the water and ammonia interactions with active sites, we find that an increase in solvent coordination to the Cu-active sites liberates the Cu species away from the CHA framework. DRIFTS data showed the formation and consumption of short-lived intermediates in the catalytic reaction, crucially, the detection of important bands for both nitrosamine and bidentate nitrate species, which is in accordance with the calculated frequencies by QM/MM calculation, giving further credence to the proposed mechanism. Our computational analysis provides a clear assignment of all main spectroscopic features of the NH_3-SCR catalytic cycle, which are in good agreement with experiment. To understand the role of solvents on the kinetics of the NH_3-SCR cycle, the adsorption of gaseous species and the formation of intermediates and their spectroscopic signatures on the solvated active sites have been investigated which can help tune the rational design of important reaction steps. From the potential energy landscapes, we observed that the formation of nitrate species is energetically more favorable on solvated active sites than on the bare site, suggesting that solvents can promote the re-oxidation part of the NH_3-SCR cycle. This

https://doi.org/10.1021/jacs.2c09823
J. Am. Chem. Soc. 2023, 145, 247−259

effect is more significant in the case of water than ammonia. In contrast to the potential benefits seen on the oxidative part, both water and ammonia are found to inhibit the reduction part of SCR since the formation of important intermediates such as Cu-nitrosamine is relatively less favorable on solvated active sites than on the bare sites, suggesting that solvent can slow down the reduction part of the NH_3-SCR cycle. This finding explains why there is some debate concerning the effect of water and ammonia on the reaction since it seems to affect some parts of the cycle positively and others negatively. In addition, solvating ammonia species were also found to accelerate the oxidation part of the cycle, which is also apparently evident from experimental data showing that preadsorbed NH_3 at 250−300 °C can enhance the NOx reduction. Our study provides additional understanding, helping to unravel the influence of solvents on the energetics of the active sites, and provides guidance for optimizing the NH_3-SCR process.

■ ASSOCIATED CONTENT

Supporting Information

The Supporting Information is available free of charge at https://pubs.acs.org/doi/10.1021/jacs.2c09823.

Additional computational details; benchmarking studies; vibrational calculations and scaling study; characterization details of prepared Cu-CHA zeolite; potential reaction-energy landscape for all three active sites; and binding energy study of HONO species (PDF)

■ AUTHOR INFORMATION

Corresponding Authors

Jamal Abdul Nasir − *Department of Chemistry, Kathleen Lonsdale Materials Chemistry, University College London, London WC1H 0AJ, U.K.;* orcid.org/0000-0002-0474-1610; Email: jamal.nasir.18@ucl.ac.uk

C. Richard A. Catlow − *Department of Chemistry, Kathleen Lonsdale Materials Chemistry, University College London, London WC1H 0AJ, U.K.; UK Catalysis Hub, Research Complex at Harwell, Rutherford Appleton Laboratory, Oxfordshire OX11 0FA, U.K.; School of Chemistry, Cardiff University, Cardiff CF10 3AT, U.K.;* orcid.org/0000-0002-1341-1541; Email: c.r.a.catlow@ucl.ac.uk

Alexey A. Sokol − *Department of Chemistry, Kathleen Lonsdale Materials Chemistry, University College London, London WC1H 0AJ, U.K.;* orcid.org/0000-0003-0178-1147; Email: a.sokol@ucl.ac.uk

Authors

Jingcheng Guan − *Department of Chemistry, Kathleen Lonsdale Materials Chemistry, University College London, London WC1H 0AJ, U.K.*

Thomas W. Keal − *Scientific Computing Department, STFC Daresbury Laboratory, Warrington WA4 4AD, U.K.;* orcid.org/0000-0001-8747-3975

Alec W. Desmoutier − *Department of Chemistry, Kathleen Lonsdale Materials Chemistry, University College London, London WC1H 0AJ, U.K.*

You Lu − *Scientific Computing Department, STFC Daresbury Laboratory, Warrington WA4 4AD, U.K.;* orcid.org/0000-0002-7524-4179

Andrew M. Beale − *Department of Chemistry, Christopher Ingold Building, University College London, London WC1H 0AJ, U.K.; UK Catalysis Hub, Research Complex at Harwell, Rutherford Appleton Laboratory, Oxfordshire OX11 0FA, U.K.;* orcid.org/0000-0002-0923-1433

Complete contact information is available at: https://pubs.acs.org/10.1021/jacs.2c09823

Author Contributions

The manuscript was written through contributions of all authors. All authors have given approval to the final version of the manuscript.

Funding

We would like to acknowledge the financial support for Jamal Abdul Nasir's study from the Project Management Unit (PMU) Higher Education Department of KPK, Pakistan, and the financial support from the EPSRC.

Notes

The authors declare no competing financial interest.

■ ACKNOWLEDGMENTS

The authors wish to acknowledge support from the EPSRC grants EP/R001847/1 and EP/W014580/1 and the UK Catalysis Hub funded by EPSRC grants EP/R026939/1 and EP/R026815/1. We also wish to acknowledge the MCC grant EP/R029431/1 and computational support provided by CoSeC, the Computational Science Centre for Research Communities, through the MCC. We also thank the UCL research computing facilities, the ISIS materials characterisation laboratory for access to the X-ray diffractometer, I. Lezcano-Gonzalez for preparing the Cu-SSZ-13 samples and A. G. Greenaway, A. Marberger, and D. Ferri for the collection and processing of the DRIFTS data.

■ ABBREVIATIONS

SCR	selective catalytic reduction
QM/MM	quantum mechanical/molecular mechanical
DFT	density functional theory
CHA	chabazite
DRIFTS	Diffuse Reflectance Infrared Fourier-Transform Spectroscopy
FTIR	Fourier transform infrared
MD	molecular dynamics
AIMD	*ab initio* molecular dynamics
PXRD	powder X-ray diffraction
EDX	energy-dispersive X-ray
BET	Brunauer−Emmett−Teller
MES	modulation excitation spectroscopy
PSD	phase-sensitive detection

■ REFERENCES

(1) Skalska, K.; Miller, J. S.; Ledakowicz, S. Trends in NO abatement: A review. *Sci. Total Environ.* **2010**, *408*, 3976−3989.

(2) Beale, A. M.; Gao, F.; Lezcano-Gonzalez, I.; Peden, C. H.; Szanyi, J. Recent advances in automotive catalysis for NOx emission control by small-pore microporous materials. *Chem. Soc. Rev.* **2015**, *44*, 7371−7405.

(3) Horowitz, L. W.; Jacob, D. J. Global impact of fossil fuel combustion on atmospheric NOx. *J. Geophys. Res. Atmos.* **1999**, *104*, 23823−23840.

(4) Damma, D.; Ettireddy, P. R.; Reddy, B. M.; Smirniotis, P. G. A review of low temperature NH3-SCR for removal of NOx. *Catalysts* **2019**, *9*, 349.

(5) Brandenberger, S.; Kröcher, O.; Tissler, A.; Althoff, R. The State of the Art in Selective Catalytic Reduction of NOxby Ammonia Using Metal-Exchanged Zeolite Catalysts. *Catal. Rev.* **2008**, *50*, 492−531.
(6) Koebel, M.; Elsener, M.; Kleemann, M. Urea-SCR: a promising technique to reduce NOx emissions from automotive diesel engines. *Catal. Today* **2000**, *59*, 335−345.
(7) Deka, U.; Juhin, A.; Eilertsen, E. A.; Emerich, H.; Green, M. A.; Korhonen, S. T.; Weckhuysen, B. M.; Beale, A. M. Confirmation of isolated Cu2+ ions in SSZ-13 zeolite as active sites in NH3-selective catalytic reduction. *J. Phys. Chem. C* **2012**, *116*, 4809−4818.
(8) Ma, L.; Cheng, Y.; Cavataio, G.; McCabe, R. W.; Fu, L.; Li, J. Characterization of commercial Cu-SSZ-13 and Cu-SAPO-34 catalysts with hydrothermal treatment for NH3-SCR of NOx in diesel exhaust. *Chem. Eng. J.* **2013**, *225*, 323−330.
(9) Marberger, A.; Petrov, A. W.; Steiger, P.; Elsener, M.; Kröcher, O.; Nachtegaal, M.; Ferri, D. Time-resolved copper speciation during selective catalytic reduction of NO on Cu-SSZ-13. *Nat. Catal.* **2018**, *1*, 221−227.
(10) Paolucci, C.; Khurana, I.; Parekh, A. A.; Li, S.; Shih, A. J.; Li, H.; Di Iorio, J. R.; Albarracin-Caballero, J. D.; Yezerets, A.; Miller, J. T.; Delgass, W. N.; Ribeiro, F. H.; Schneider, W. F.; Gounder, R. Dynamic multinuclear sites formed by mobilized copper ions in NO x selective catalytic reduction. *Science* **2017**, *357*, 898−903.
(11) Millan, R.; Cnudde, P.; van Speybroeck, V.; Boronat, M. Mobility and Reactivity of Cu+ Species in Cu-CHA Catalysts under NH3-SCR-NOx Reaction Conditions: Insights from AIMD Simulations. *JACS Au* **2021**, *1*, 1778−1787.
(12) Janssens, T. V.; Falsig, H.; Lundegaard, L. F.; Vennestrøm, P. N.; Rasmussen, S. B.; Moses, P. G.; Giordanino, F.; Borfecchia, E.; Lomachenko, K. A.; Lamberti, C.; Bordiga, S.; Godiksen, A.; Mossin, S.; Beato, P. A consistent reaction scheme for the selective catalytic reduction of nitrogen oxides with ammonia. *ACS Catal.* **2015**, *5*, 2832−2845.
(13) Akter, N.; Chen, X.; Parise, J.; Boscoboinik, J. A.; Kim, T. Effects of copper loading on NH3-SCR and NO oxidation over Cu impregnated CHA zeolite. *Korean J. Chem. Eng.* **2018**, *35*, 89−98.
(14) Wallin, M.; Karlsson, C.-J.; Skoglundh, M.; Palmqvist, A. Selective catalytic reduction of NOx with NH3 over zeolite H-ZSM-5: influence of transient ammonia supply. *J. Catal.* **2003**, *218*, 354−364.
(15) Liu, Y.; Xue, W.; Seo, S.; Tan, X.; Mei, D.; Liu, C.-j.; Nam, I.-S.; Hong, S. B. Water: A promoter of ammonia selective catalytic reduction over copper-exchanged LTA zeolites. *Appl. Catal., B* **2021**, *294*, 120244.
(16) Yu, T.; Wang, J.; Shen, M.; Wang, J.; Li, W. The influence of CO2 and H2O on selective catalytic reduction of NO by NH3 over Cu/SAPO-34 catalyst. *Chem. Eng. J.* **2015**, *264*, 845−855.
(17) Lee, H.; Song, I.; Jeon, S. W.; Kim, D. H. Mobility of Cu Ions in Cu-SSZ-13 Determines the Reactivity of Selective Catalytic Reduction of NOx with NH3. *J. Phys. Chem. Lett.* **2021**, *12*, 3210−3216.
(18) Wan, Y.; Yang, G.; Xiang, J.; Shen, X.; Yang, D.; Chen, Y.; Rac, V.; Rakic, V.; Du, X. Promoting effects of water on the NH3-SCR reaction over Cu-SAPO-34 catalysts: transient and permanent influences on Cu species. *Dalton Trans.* **2020**, *49*, 764−773.
(19) O'Malley, A. J.; Hitchcock, I.; Sarwar, M.; Silverwood, I. P.; Hindocha, S.; Catlow, C. R. A.; York, A. P.; Collier, P. Ammonia mobility in chabazite: insight into the diffusion component of the NH3-SCR process. *Phys. Chem. Chem. Phys.* **2016**, *18*, 17159−17168.
(20) Hu, W.; Selleri, T.; Gramigni, F.; Fenes, E.; Rout, K. R.; Liu, S.; Nova, I.; Chen, D.; Gao, X.; Tronconi, E. On the Redox Mechanism of Low-Temperature NH 3 -SCR over Cu-CHA: A Combined Experimental and Theoretical Study of the Reduction Half Cycle. *Angew. Chem.* **2021**, *133*, 7273−7280.
(21) Ruggeri, M. P.; Nova, I.; Tronconi, E. Experimental study of the NO oxidation to NO 2 over metal promoted zeolites aimed at the identification of the standard SCR rate determining step. *Top. Catal.* **2013**, *56*, 109−113.
(22) Catlow, C. R. A.; Buckeridge, J.; Farrow, M. R.; Logsdail, A. J.; Sokol, A. A.Quantum Mechanical/Molecular Mechanical (QM/MM) Approaches. In *Handbook of Solid State Chemistry*; Dronskowski, R., Kikkawa, S., Stein, A., Eds.; Wiley-VCH, 2017; Vol. *5*, pp 647−680.
(23) Sherwood, P.; de Vries, A. H.; Collins, S. J.; Greatbanks, S. P.; Burton, N. A.; Vincent, M. A.; Hillier, I. H. Computer simulation of zeolite structure and reactivity using embedded cluster methods. *Faraday Discuss.* **1997**, *106*, 79−92.
(24) Metz, S.; Kästner, J.; Sokol, A. A.; Keal, T. W.; Sherwood, P. C hem S hell-a modular software package for QM / MM simulations. *Wiley Interdiscip. Rev.: Comput. Mol. Sci.* **2014**, *4*, 101−110.
(25) Lu, Y.; Farrow, M. R.; Fayon, P.; Logsdail, A. J.; Sokol, A. A.; Catlow, C. R. A.; Sherwood, P.; Keal, T. W. Open-Source, python-based redevelopment of the ChemShell multiscale QM/MM environment. *J. Chem. Theor. Comput.* **2018**, *15*, 1317−1328.
(26) Sherwood, P.; de Vries, A. H.; Guest, M. F.; Schreckenbach, G.; Catlow, C. R. A.; French, S. A.; Sokol, A. A.; Bromley, S. T.; Thiel, W.; Turner, A. J. QUASI: A general purpose implementation of the QM/MM approach and its application to problems in catalysis. *J. Mol. Struct.: THEOCHEM* **2003**, *632*, 1−28.
(27) Guest, M. F.; Bush, I. J.; Van Dam, H. J. J.; Sherwood, P.; Thomas, J. M. H.; Van Lenthe, J. H.; Havenith, R. W. A.; Kendrick, J. The GAMESS-UK electronic structure package: algorithms, developments and applications. *Mol. Phys.* **2005**, *103*, 719−747.
(28) Smith, W.; Yong, C.; Rodger, P. DL_POLY: Application to molecular simulation. *Mol. Simul.* **2002**, *28*, 385−471.
(29) Hill, J. R.; Sauer, J. Molecular mechanics potential for silica and zeolite catalysts based on ab initio calculations. 1. Dense and microporous silica. *J. Phys. Chem.* **1994**, *98*, 1238−1244.
(30) Weigend, F.; Ahlrichs, R. Balanced basis sets of split valence, triple zeta valence and quadruple zeta valence quality for H to Rn: Design and assessment of accuracy. *Phys. Chem. Chem. Phys.* **2005**, *7*, 3297−3305.
(31) Wilson, P. J.; Bradley, T. J.; Tozer, D. J. Hybrid exchange-correlation functional determined from thermochemical data and ab initio potentials. *J. Chem. Phys.* **2001**, *115*, 9233−9242.
(32) Janssens, T. V.; Falsig, H.; Lundegaard, L. F.; Vennestrøm, P. N.; Rasmussen, S. B.; Moses, P. G.; Giordanino, F.; Borfecchia, E.; Lomachenko, K. A.; Lamberti, C.; Bordiga, S.; Godiksen, A.; Mossin, S.; Beato, P. A consistent reaction scheme for the selective catalytic reduction of nitrogen oxides with ammonia. *ACS Catal.* **2015**, *5*, 2832−2845.
(33) Dent, L.; Smith, J. Crystal structure of chabazite, a molecular sieve. *Nature* **1958**, *181*, 1794−1796.
(34) Gale, J. D.; Rohl, A. L. The general utility lattice program (GULP). *Mol. Simul.* **2003**, *29*, 291−341.
(35) Sherwood, P.; de Vries, A. H.; Collins, S. J.; Greatbanks, S. P.; Burton, N. A.; Vincent, M. A.; Hillier, I. H. Computer simulation of zeolite structure and reactivity using embedded cluster methods. *Faraday Discuss.* **1997**, *106*, 79−92.
(36) Zhao, Y.; Lynch, B. J.; Truhlar, D. G. Development and assessment of a new hybrid density functional model for thermochemical kinetics. *J. Phys. Chem. A* **2004**, *108*, 2715−2719.
(37) Greenaway, A. G.; Lezcano-Gonzalez, I.; Agote-Aran, M.; Gibson, E. K.; Odarchenko, Y.; Beale, A. M. Operando Spectroscopic Studies of Cu−SSZ-13 for NH3−SCR deNOx Investigates the Role of NH3 in Observed Cu (II) Reduction at High NO Conversions. *Top. Catal.* **2018**, *61*, 175−182.
(38) Greenaway, A. G.; Marberger, A.; Thetford, A.; Lezcano-González, I.; Agote-Arán, M.; Nachtegaal, M.; Ferri, D.; Kröcher, O.; Catlow, C. R. A.; Beale, A. M. Detection of key transient Cu intermediates in SSZ-13 during NH3-SCR deNOx by modulation excitation IR spectroscopy. *Chem. Sci.* **2020**, *11*, 447−455.
(39) Haszeldine, R.; Jander, J. Further remarks on the spectra of nitrites and nitrosamines. *J. Chem. Phys.* **1955**, *23*, 979−980.
(40) Piskorz, M.; Urbanski, T. Ultraviolet and infrared spectra of some nitrosamines. *Bull. Acad. Pol. Sci., Ser. Sci. Chim.* **1963**, *11*, 607−613.
(41) Tarte, P. Recherches spectroscopiques sur les composés nitrosés. *Bull. Soc. Chim. Belg.* **1954**, *63*, 525−541.

https://doi.org/10.1021/jacs.2c09823
J. Am. Chem. Soc. 2023, 145, 247−259

(42) Kedrova, T.; Gafurov, R.; Sogomonyan, E.; Eremenko, L. Spectroscopic study of (nitroalkyl)nitrosamines. *Bull. Acad. Sci. USSR, Div. Chem. Sci.* **1979**, *28*, 944−947.
(43) Zapata, F.; García-Ruiz, C. The discrimination of 72 nitrate, chlorate and perchlorate salts using IR and Raman spectroscopy. *Spectrochim. Acta, Part A* **2018**, *189*, 535−542.
(44) Volod'ko, L.; Huoah, L. T. The vibrational spectra of aqueous nitrate solutions. *J. Appl. Spectrosc.* **1968**, *9*, 1100−1104.
(45) Bordiga, S.; Lamberti, C.; Bonino, F.; Travert, A.; Thibault-Starzyk, F. Probing zeolites by vibrational spectroscopies. *Chem. Soc. Rev.* **2015**, *44*, 7262−7341.
(46) Negri, C.; Hammershøi, P. S.; Janssens, T. V.; Beato, P.; Berlier, G.; Bordiga, S. Investigating the Low Temperature Formation of Cu II -(N,O) Species on Cu-CHA Zeolites for the Selective Catalytic Reduction of NO x. *Chem.—Eur. J.* **2018**, *24*, 12044−12053.
(47) Hadjiivanov, K. I. Identification of neutral and charged N x O y surface species by IR spectroscopy. *Catal. Rev.* **2000**, *42*, 71−144.
(48) Yao, X.; Ma, K.; Zou, W.; He, S.; An, J.; Yang, F.; Dong, L. Influence of preparation methods on the physicochemical properties and catalytic performance of MnO -CeO2 catalysts for NH3-SCR at low temperature. *Chin. J. Catal.* **2017**, *38*, 146−159.
(49) Giordanino, F.; Borfecchia, E.; Lomachenko, K. A.; Lazzarini, A.; Agostini, G.; Gallo, E.; Soldatov, A. V.; Beato, P.; Bordiga, S.; Lamberti, C. Interaction of NH3 with Cu-SSZ-13 catalyst: a complementary FTIR, XANES, and XES study. *J. Phys. Chem. Lett.* **2014**, *5*, 1552−1559.
(50) Lezcano-Gonzalez, I.; Deka, U.; Arstad, B.; Van Yperen-De Deyne, A.; Hemelsoet, K.; Waroquier, M.; Van Speybroeck, V.; Weckhuysen, B. M.; Beale, A. M. Determining the storage, availability and reactivity of NH3within Cu-Chabazite-based Ammonia Selective Catalytic Reduction systems. *Phys. Chem. Chem. Phys.* **2014**, *16*, 1639−1650.
(51) Paolucci, C.; Khurana, I.; Parekh, A. A.; Li, S.; Shih, A. J.; Li, H.; Di Iorio, J. R.; Albarracin-Caballero, J. D.; Yezerets, A.; Miller, J. T.; Delgass, W. N.; Ribeiro, F. H.; Schneider, W. F.; Gounder, R. Dynamic multinuclear sites formed by mobilized copper ions in NO x selective catalytic reduction. *Science* **2017**, *357*, 898−903.
(52) Millan, R.; Cnudde, P.; Hoffman, A. E.; Lopes, C. W.; Concepción, P.; van Speybroeck, V.; Boronat, M. Theoretical and Spectroscopic Evidence of the Dynamic Nature of Copper Active Sites in Cu-CHA Catalysts under Selective Catalytic Reduction (NH3-SCR-NOx) Conditions. *J. Phys. Chem. Lett.* **2020**, *11*, 10060−10066.
(53) Gao, F.; Mei, D.; Wang, Y.; Szanyi, J.; Peden, C. H. Selective Catalytic Reduction over Cu/SSZ-13: Linking Homo- and Heterogeneous Catalysis. *J. Am. Chem. Soc.* **2017**, *139*, 4935−4942.
(54) Chen, L.; Falsig, H.; Janssens, T. V.; Grönbeck, H. Activation of oxygen on (NH3Cu NH3)+ in NH3-SCR over Cu-CHA. *J. Catal.* **2018**, *358*, 179−186.
(55) Moreno-González, M.; Millán, R.; Concepción, P.; Blasco, T.; Boronat, M. Spectroscopic Evidence and Density Functional Theory (DFT) Analysis of Low-Temperature Oxidation of Cu+ to Cu2+ NO x in Cu-CHA Catalysts: Implications for the SCR-NO x Reaction Mechanism. *ACS Catal.* **2019**, *9*, 2725−2738.
(56) Wilken, N.; Kamasamudram, K.; Currier, N. W.; Li, J.; Yezerets, A.; Olsson, L. Heat of adsorption for NH3, NO2 and NO on Cu-Beta zeolite using microcalorimeter for NH3 SCR applications. *Catal. Today* **2010**, *151*, 237−243.
(57) Olsson, L.; Wijayanti, K.; Leistner, K.; Kumar, A.; Joshi, S. Y.; Kamasamudram, K.; Currier, N. W.; Yezerets, A. A multi-site kinetic model for NH3-SCR over Cu/SSZ-13. *Appl. Catal., B* **2015**, *174−175*, 212−224.
(58) Krossner, M.; Sauer, J. Interaction of Water with Brønsted Acidic Sites of Zeolite Catalysts. Ab Initio Study of 1:1 and 2:1 Surface Complexes. *J. Phys. Chem.* **1996**, *100*, 6199−6211.
(59) Jobic, H.; Tuel, A.; Krossner, M.; Sauer, J. Water in interaction with acid sites in H-ZSM-5 zeolite does not form hydroxonium ions. A comparison between neutron scattering results and ab initio calculations. *J. Phys. Chem.* **1996**, *100*, 19545−19550.
(60) Parrillo, D.; Lee, C.; Gorte, R. Heats of adsorption for ammonia and pyridine in H-ZSM-5: evidence for identical Brønsted-acid sites. *Appl. Catal., A* **1994**, *110*, 67−74.
(61) Mei, D.; Lercher, J. A. Mechanistic insights into aqueous phase propanol dehydration in H-ZSM-5 zeolite. *AIChE J.* **2017**, *63*, 172−184.
(62) Tuma, C.; Sauer, J. A hybrid MP2/planewave-DFT scheme for large chemical systems: proton jumps in zeolites. *Chem. Phys. Lett.* **2004**, *387*, 388−394.
(63) Gao, F.; Kwak, J. H.; Szanyi, J.; Peden, C. H. Current understanding of Cu-exchanged chabazite molecular sieves for use as commercial diesel engine DeNO x catalysts. *Top. Catal.* **2013**, *56*, 1441−1459.
(64) Bendrich, M.; Scheuer, A.; Hayes, R.; Votsmeier, M. Unified mechanistic model for Standard SCR, Fast SCR, and NO 2 SCR over a copper chabazite catalyst. *Appl. Catal., B* **2018**, *222*, 76−87.
(65) Borfecchia, E.; Lomachenko, K.; Giordanino, F.; Falsig, H.; Beato, P.; Soldatov, A.; Bordiga, S.; Lamberti, C. Revisiting the nature of Cu sites in the activated Cu-SSZ-13 catalyst for SCR reaction. *Chem. Sci.* **2015**, *6*, 548−563.
(66) Bordiga, S.; Lamberti, C.; Bonino, F.; Travert, A.; Thibault-Starzyk, F. Probing zeolites by vibrational spectroscopies. *Chem. Soc. Rev.* **2015**, *44*, 7262−7341.
(67) Soyer, S.; Uzun, A.; Senkan, S.; Onal, I. A quantum chemical study of nitric oxide reduction by ammonia (SCR reaction) on V2O5 catalyst surface. *Catal. Today* **2006**, *118*, 268−278.
(68) Walch, S. P. Theoretical characterization of the reaction NH2+NO→products. *J. Chem. Phys.* **1993**, *99*, 5295−5300.
(69) Sun, D.; Schneider, W. F.; Adams, J. B.; Sengupta, D. Molecular Origins of Selectivity in the Reduction of NOx by NH3. *J. Phys. Chem. A* **2004**, *108*, 9365−9374.
(70) Anstrom, M.; Topsøe, N.-Y.; Dumesic, J. Density functional theory studies of mechanistic aspects of the SCR reaction on vanadium oxide catalysts. *J. Catal.* **2003**, *213*, 115−125.
(71) Gilardoni, F.; Bell, A. T.; Chakraborty, A.; Boulet, P. Density Functional Theory Calculations of the Oxidative Dehydrogenation of Propane on the (010) Surface of V2O5†. *J. Phys. Chem. B* **2000**, *104*, 12250−12255.
(72) Chen, L.; Janssens, T. V.; Vennestrøm, P. N.; Jansson, J.; Skoglundh, M.; Grönbeck, H. A complete multisite reaction mechanism for low-temperature NH3-SCR over Cu-CHA. *ACS Catal.* **2020**, *10*, 5646−5656.
(73) Mao, Y.; Wang, Z.; Wang, H.-F.; Hu, P. Understanding Catalytic Reactions over Zeolites: A Density Functional Theory Study of Selective Catalytic Reduction of NOx by NH3 over Cu-SAPO-34. *ACS Catal.* **2016**, *6*, 7882−7891.
(74) Li, J.; Li, S. New insight into selective catalytic reduction of nitrogen oxides by ammonia over H-form zeolites: a theoretical study. *Phys. Chem. Chem. Phys.* **2007**, *9*, 3304−3311.
(75) Brüggemann, T. C.; Keil, F. J. Theoretical investigation of the mechanism of the selective catalytic reduction of nitric oxide with ammonia on H-form zeolites. *J. Phys. Chem. C* **2008**, *112*, 17378−17387.
(76) Usberti, N.; Gramigni, F.; Nasello, N. D.; Iacobone, U.; Selleri, T.; Hu, W.; Liu, S.; Gao, X.; Nova, I.; Tronconi, E. An experimental and modelling study of the reactivity of adsorbed NH3 in the low temperature NH3-SCR reduction half-cycle over a Cu-CHA catalyst. *Appl. Catal., B* **2020**, *279*, 119397.

https://doi.org/10.1021/jacs.2c09823
J. Am. Chem. Soc. 2023, 145, 247−259